Regular Article

# Bouncing bubbles do not show water slip on smooth hydrophobic surfaces

Ivan U. Vakarelski [a,b,*], Farrukh Kamoliddinov [a], Sigurdur T. Thoroddsen [a]

[a] Division of Physical Sciences and Engineering, King Abdullah University of Science and Technology (KAUST), Thuwal 23955-6900, Saudi Arabia
[b] Department of Chemical and Pharmaceutical Engineering, Faculty of Chemistry and Pharmacy, Sofia University, 1 James Bourchier Avenue, 1164 Sofia, Bulgaria

HIGHLIGHTS

- Bubbles bounce stronger from mobile (free-slip) than immobile (no-slip) interfaces.
- Bubbles in water bounce identically from hydrophobic and hydrophilic substrates.
- Bubbles bounce from solid in water agrees with no-slip wall numerical simulations.
- The no-slip boundary condition holds for bubble bounce from hydrophobic surfaces.

GRAPHICAL ABSTRACT
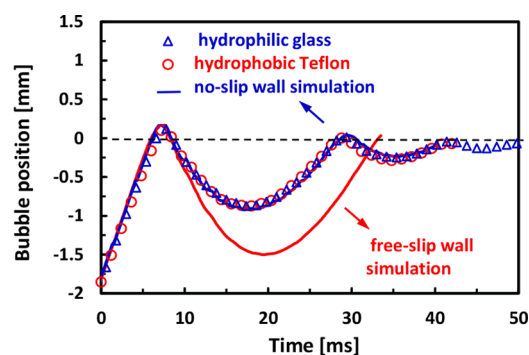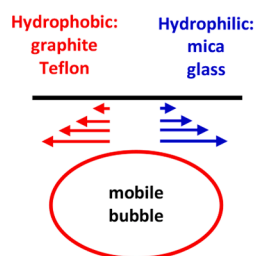
ABSTRACT

Hypothesis: The presence of hydrodynamic slip of water on smooth hydrophobic surfaces has been debated intensely over the last decades. In recent experiments, the stronger bounce of free-rising bubbles from smooth hydrophobic surfaces compared to smooth hydrophilic surfaces was interpreted as evidence for a significant water slip on smooth hydrophobic surfaces.

Experiments: To examine the possible water-slip effect, we conduct well-controlled experiments comparing the bouncing dynamics of millimeter-sized free-rising bubbles from smooth hydrophobic and hydrophilic surfaces. The hydrophobic surfaces were graphite or Teflon, and the hydrophilic surfaces were glass or mica. To avoid contamination, the experiments were conducted in pure water without any surface-active additives. Numerical simulations were also used to compare the bounce of the bubble from a no-slip and free-slip walls.

Finding: Our experiments show that the free-rising bubbles in pure water bounce identically from the smooth hydrophobic graphite or Teflon surfaces as from smooth hydrophilic mica or glass surfaces. The bubble bounce from all four surfaces is in excellent agreement with the numerical simulation of a bubble bouncing from a flat, no-slip wall. At the same time, numerical simulations for bubbles bouncing from a free-slip wall predict up to two-fold stronger bouncing amplitudes. Our experiments and numerical simulations, including estimates of the shear rates, confirm the no-slip boundary condition for water on smooth hydrophobic surfaces.

1. Introduction

The boundary condition between a solid and a liquid, between two immiscible liquids or between a gas and a liquid, is a fundamental property that determines the fluid flow and hydrodynamic interactions in various naturally occurring and practically important colloidal systems. Examples include the interaction between deformable bubbles and droplets [1,2] as well as flow in porous media and microfluidic devices [3,4]. It is generally accepted that the fluid molecules in contact with solid interfaces move with the same velocity as the solid in tangential and normal directions. This is the no-slip boundary condition. The tangential velocity between two immiscible fluids is determined by the ratio of the fluids' viscosities. Due to the significant difference in viscosity between a gas and a liquid, a clean gas–liquid interface is unable to sustain tangential stress and is expected to be tangentially mobile. Such interfaces are referred to as tangentially mobile or simply mobile fluid interfaces. In practical situations, surface-active contaminants or the addition of surfactants can immobilize the gas–liquid or liquid–liquid interface due to Marangoni-stress effects [5,6]. Such fluid interfaces are referred to as tangentially immobile or immobile fluid interfaces (no-slip).

For the case of fluid flow in confined spaces, the no-slip boundary condition has been challenged by a slip boundary condition, which assumes that there can be a finite tangential velocity of the liquid adjusted to the solid wall. One common phenomenological model to characterize slip is the use of the Navier condition that relates the tangential fluid velocity at a solid boundary to the tangential derivative of the fluid velocity in terms of the slip length parameter. This condition is given as $u_x^0 = b(du_x/dy)|_{y=0}$, where u_x^0 is the fluid tangential velocity near the interface, (du_x/dy) is the velocity gradient in normal direction to the interface and b is a phenomenological parameter known as the Navier slip-length, used to parametrized slip (see schematics in Fig. 1). In the case of water, slip is expected to be more significant over a smooth hydrophobic surface than a smooth hydrophilic surface. The existence and the magnitude of the slip of water on smooth hydrophilic or hydrophobic surfaces has been debated in the literature over the last decades [7–17]. A major part of the experimental evidence comes from atomic force microscopy (AFM) colloidal probe experiments. At the same time, it is recognized that the accuracy of such experiments can be affected by multiple factors, and the measured slip lengths, ranging from few to tens of nanometres, often are within the limit of the experimental error [11,12,17]. One of the latest AFM investigations shows no measurable slip on smooth hydrophilic and hydrophobic surfaces and discusses possible artifacts [17].

We note that apart from the "true slip" of liquids over solids discussed here, the Navier slip length concept is often used as an apparent slip length, which subsumes effects related to the surface's roughness [18,19], the presence of nano-bubbles on hydrophobic surfaces, or thin gas layer (plastron) sustained on superhydrophobic surfaces [20–22].

In our recent studies, we have demonstrated an alternative way of determining the mobility of liquid interfaces, by observing the bouncing dynamics of free-rising millimetre-sized bubbles in liquids. Bubbles in an ultrapure fluorocarbon liquid or pure water bounce significantly stronger from a mobile than an immobile fluid interface (up to twice-as-large bouncing distance) [23–25]. The stronger bounce was explained by lower viscous losses in the flow around the bubble during its bounce from a mobile fluid interface than the immobile fluid interface. Numerical simulations suggest that the same effect should be observed for a bubble bouncing from a flat solid interface, with a bubble bouncing stronger from a mobile or free-slip flat solid than from a no-slip flat solid. [23,26].

More recently, Pawliszak et al. studied the bouncing of free-rising bubbles in water from a smooth graphite substrate, the hydrophobicity of which was modified by the adsorption of surface-active biopolymers [27]. They found that bubbles bounced more strongly from the unmodified hydrophobic graphite or Teflon substrate compared to the bouncing from graphite substrates modified by biopolymer adsorption. The more than two-fold stronger bouncing amplitude from the hydrophobic substrates compared to the hydrophilic substrate, was in this study interpreted as evidence of a significant water slip on the smooth hydrophobic surfaces during the bubble bounce.

Here, to test the claims for water slipping in bubble bouncing experiments, we aim to conduct well-controlled free-rising bubbles bouncing from smooth hydrophilic and smooth hydrophobic surfaces experiments. As in the study of Pawliszak et al. [27], we use molecularly smooth Highly Oriented Pyrolytic Graphite (HOPG) as well as polytetrafluoroethylene (PTFE, commercially known as Teflon) as hydrophobic surfaces. To avoid any possible contamination from surface-active components, here as hydrophilic substrates, we use flat glass slides or molecularly-smooth mica samples. Another important point to clarify is that the majority of prior studies investigated slip on substrates rendered hydrophobic through the deposition of silane monolayers or hydrophobic polymers, which may exhibit more complex hydrodynamic behaviour [9–19]. In the present work, as in Pawliszak et al., we consider only smooth unmodified solid surface of high hydrophobicity, such as graphite and Teflon.

First, we will briefly review experiments on the bubble bounces from mobile and immobile water–air interfaces, that demonstrate the effects of interface mobility on the bouncing dynamics. Next, we will compare the bubbles in water bouncing from the two hydrophilic and two hydrophobic substrates and numerical simulation of the same bubble bounces from the no-slip and free-slip solid interfaces. Finally, we will use the simulation results to estimate the shear rates on the substrates during the bubble bounce and how they compare to prior investigations estimated slip length shear rate dependencies.

2. Experimental methods and numerics

2.1. Hydrophilic and hydrophobic substrates

We studied the bouncing of free-rising bubbles in water against four different substrates to contrast how they bounce from smooth hydrophilic and hydrophobic surfaces. The hydrophilic substrates were glass and mica, and the hydrophobic substrates were polytetrafluoroethylene (PTFE) and Highly Ordered Pyrolytic Graphite (HOPG). The glass substrates were Fisher cover glass slides. The mica, HOPG, and PTFE samples were all purchased from SPI® Supplies. The mica samples were SPI-Chem Mica Grade V-1, and the HOPG samples were SPI-1 Grade. The PTFE samples were prepared from SPI supplied by PTFE Beaker Covers.

The surface roughness of the samples was evaluated by atomic force microscopy (AFM) imaging (Supplementary Fig. S1). As expected, the freshly cleaved mica and HOPG are molecularly smooth with an RMS of less than 0.1 nm. The glass substrates were also very smooth, with an RMS of about 0.3 nm over a 1 μm^2 area. The PTFE samples were
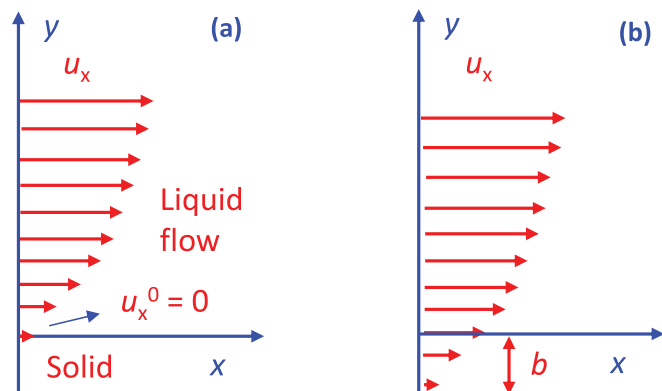

Fig. 1. Schematic representation of the solid–liquid interface (a) no-slip boundary condition and (b) slip boundary conditions with a slip length b.

flattened by compressing them against a freshly cleaved mica surface and heating them to about 280 °C for 24 h [28]. This resulted in smoothing of the PTFE surface to an RMS of about 4.5 nm over a 1 μm² area.

Following the washing of the glass surface with acetone, water, and mild plasma cleaning, it becomes hydrophilic with apparent water contact angles of less than 10°. The freshly cleaved mica surface is hydrophilic and has apparent water contact angles of less than 10°. The flattened PTFE samples have the largest water contact angles, reaching 120°. The apparent water contact angle on the freshly cleaved HOPG samples is about 90°. An alternative way to demonstrate the substrates hydrophobicity is by the contact angle of the air bubbles following coalescence with the interface, as shown in Supplementary Fig. S2a for the PTFE sample and Supplementary Fig. S2b for the HOPG sample. In contrast, the bubble sits on the glass or mica surfaces without coalescing for a longer time (seconds), as seen in Supplementary Figs. S2c and d.

2.2. Experimental setup and protocol

The experimental setup we used to monitor the bubble free-rise and bouncing from the flat substrate is illustrated in Fig. 2a. This setup is essentially the same as in our earlier research on bubble dynamics in perfluorocarbon liquids and aqueous solutions [23–26]. The container was a glass cell with a cross-section of 15.0 × 5.5 cm and a height of 10.0 cm. A glass micro-capillary of 100 μm inner diameter is mounted at the bottom of the cell. By altering the air pressure feeding to the capillary, we can produce air bubbles whose diameters vary between 0.60 and 1.60 mm. The flat samples used in the study (glass, mica, PTFE, HOPG) were mounted on a vertical holder of a 3D micromanipulator, which was used to lower the samples into the water.

The bubbles' free-rise and bouncing from the flat substrates were captured using a high-speed camera (Photron-SA5) fitted with a long-distance microscope and a 5× magnification objective (Mitutoyo), achieving a resolution of 4.0 μm/pixel. The high-speed videos were recorded at a standard rate of 5000 frames per second (fps) with a shutter speed of up to 1/15000 s to minimize image smearing and ensure sharper contrast.

Before conducting the experiments, the glass vessel underwent plasma-cleaned and was rinsed with deionized water. The study focuses on bubbles with an undeformed diameter between 0.80 and 1.60 mm. The free-rising bubbles take an oblate ellipsoidal shape within this size range, as illustrated in Fig. 2b. To characterize the bubble size, we employ the equivalent diameter, $D = (D_h^2 D_v)^{1/3}$, where D_h and D_v represent the horizontal and vertical ellipsoidal diameters. The bubbles were released from a depth of more than 2.5 cm below the water–air interface to ensure they reached terminal velocity before contacting the

surface. The position of the bubble's center of mass over time, $H(t)$, was measured relative to the flat sample surface, where $H = 0$ corresponding to the undeformed bubble in contact with the sample (Fig. 2b).

Water used in our experiment was purified in a Millipore apparatus and has an internal electrical resistivity of no less than 18.4 MΩ cm. The Millipore-grade water purity ensures that the bubble rise velocities are consistent with the mobile bubble interface, over the full range of the bubble sizes used herein, $D = 0.80$ to 1.60 mm.

2.3. Gerris numerical simulations

Building on our previous studies of bubbles bouncing off interfaces in a perfluorocarbon liquid PP1, ethanol, water [23,24] and a water–glass surface [26], we performed numerical simulations using the open-source Gerris Flow Solver [29–32]. This software employs the volume-of-fluid (VOF) method to solve the incompressible Navier-Stokes equations. Its adaptability to axisymmetric geometries and use of local adaptive mesh refinement makes it highly efficient for simulating the collisions of bubbles and droplets with interfaces.

The generic Gerris code allows the implementation of both no-slip and free-slip boundary conditions at the top wall. The simulation uses the nominal physical parameters of the system: water density is 997.8 kg/m³ and water viscosity is 1.00 mPa s. Air density is 1.21 kg/m³, and viscosity 1.81×10^{-2} mP s. The water–air surface tension was set to 72.4 mN/m. All simulations start with an adaptive mesh at a refinement level of 11. As the bubble approaches and bounces off the interface, the refinement level is progressively increased to resolve the thin liquid film between the bubble and the interface. In certain cases, with a free-slip top-wall boundary condition, the adaptive mesh level is increased up to 17 to ensure adequate resolution. The simulations conducted here are identical to those in our work on bubbles bouncing from a glass surface [26] but have now been repeated using various bubble sizes. Full details on the Gerris method can be found in our prior related works [23,24,26].

3. Results and discussions

3.1. Mobility of free-rising bubbles

To correctly interpret the bouncing dynamics of the bubbles from solid interfaces, we must first evaluate the interface mobility of the free-rising bubbles in our experiments. A simple and reliable method to determine this mobility is to measure the terminal velocity of free-rising bubbles. Bubbles with mobile interfaces experience reduced viscous stress, enabling them to rise faster than those with immobilized interfaces. For the bubble size range considered in our study, the bubbles deform to take an ellipsoidal shape, and the terminal free-rise velocity of
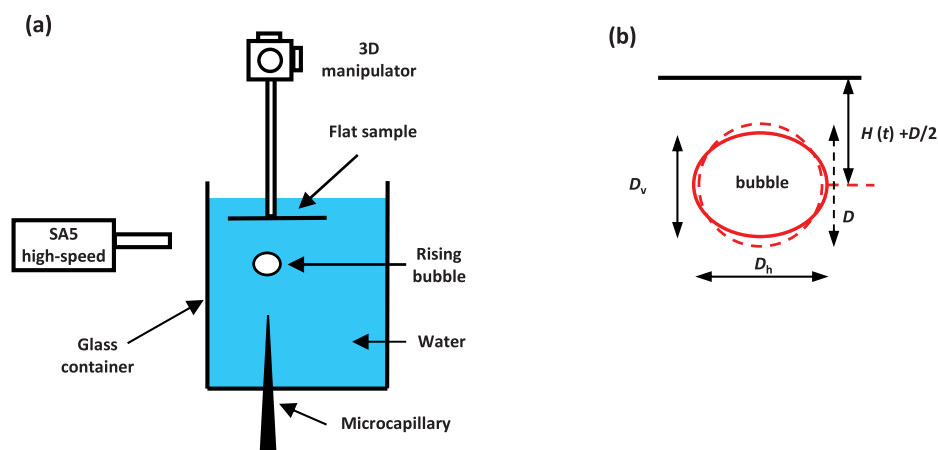

Fig. 2. (a) Schematic of the experimental setup. (b) Schematic of an oblate ellipsoidal bubble with horizontal diameter D_h and vertical diameter D_v as it approaches the flat sample.

a bubble with a mobile interface can be accurately predicted using Moore's theory for deformable bubbles at high Reynolds numbers [33,34]. However, due to Marangoni stress effects, even trace contamination can render the bubble surface partially or fully immobilized [2,35]. In the limiting case of immobile spherical bubbles at high Reynolds numbers, the terminal rise velocity is significantly lower and can be predicted by the Schiller-Naumann empirical correlation [34]. As established in prior studies, Supplementary Fig. S3 shows that for Millipore grade purity water, the free-rise velocity of bubbles of $D = 0.80$ to 1.60 mm aligns closely with Moore's theory for bubbles exhibiting a fully mobile interface [24,34].

3.2. Bubbles bouncing from mobile or immobile water–air interfaces

Assessing the mobility of the water pool interface from which a free-rising bubble bounces is more complex than determining the mobility of the free-rising bubble [24,34]. As noted in the introduction, our recent studies present an alternative method for evaluating the mobility of the pool interface by comparing the bounce dynamics of free-rising bubbles at mobile and immobile liquid interfaces [23–25]. Due to lower viscous losses, free-rising bubbles will bounce stronger from a mobile interface than from an immobile interface.

For the case of pure water in the pool, the water–air interface was made immobile by applying a Langmuir monolayer of arachidic acid (AAc) molecules [24]. The monolayer concentration is adjusted to be high enough to fully immobilize the interface without changing its surface tension. Video 1 is an example contrasting the bouncing of $D = 1.00$ mm bubble from the pure water–air interface and from a water interface immobilized with the AAc monolayer. Fig. 3 shows the bubble
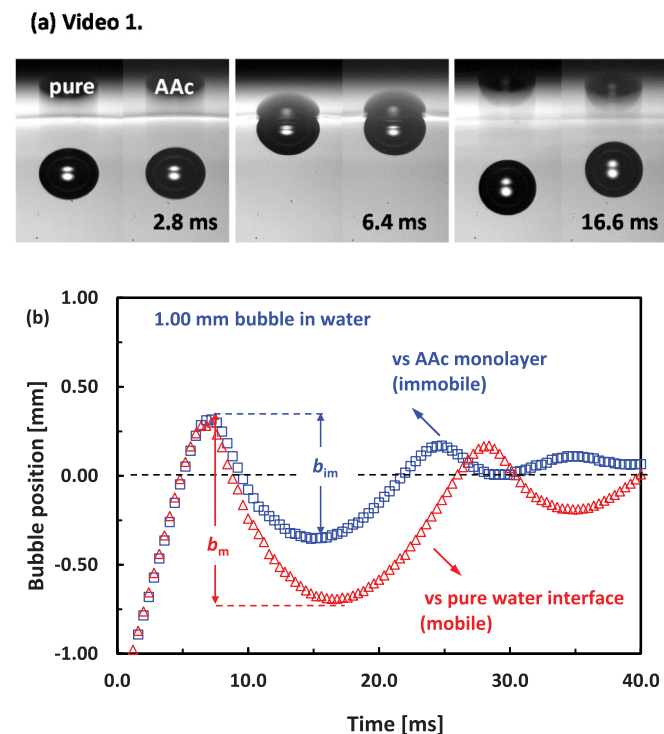
(a) Video 1.

(b)

Fig. 3. (a) High-speed camera snapshots from Video 1 showing the bounce of bubbles with a diameter of D = 1.00 mm from a pure mobile interface water pool compared to a water surface immobilized with an AAc monolayer. (b) Trajectory of the bubbles center-of-mass extracted from Video 1, for the case of bubble bouncing from the pure water–air interface (red triangles), or from the water–air interface with deposited AAc monolayer (blue squares). Figure is adopted with permission from the study of Vakarelski et al. [24]. (For interpretation of the references to color in this figure legend, the reader is referred to the web version of this article.)

center of mass *vs* time, which is extracted from these videos. As seen in Video 1 and Fig. 3, the bubble bounces significantly stronger from the mobile than from immobile water–air interface. This is quantified as the ratio of amplitudes for the first bounces, $b_m/b_{im} = 1.5$, where b_{im} is the first bounce amplitude from immobile water–air interface with the AAc deposited, and b_m is the first bounce amplitude from the mobile pure water–air interface (see Fig. 3b). A similar effect is confirmed for the entire bubble sizes range investigated, i.e. between $D = 0.80$ to 1.60 mm. The corresponding ratios of b_m/b_{im} range between 1.8 and 1.2. The full details of this investigation can be found in Vakarelski et al. [24].

3.3. Bubbles bouncing from smooth hydrophilic or hydrophobic solid surfaces

Following the study of bubbles bouncing from water-air interfaces [24], we next investigated the bouncing of free-rising bubbles from a flat glass surface in water [26]. The experimental bubble trajectories measured in this study agreed with trajectories from Gerris numerical simulations (GNS), for mobile bubbles bouncing from a no-slip solid wall. At the same time, the GNS for mobile bubbles bouncing from a free-slip wall predicted a significantly stronger bounce. In the same study, during the bubble bouncing from a glass interface, we demonstrated that the shape of the interferometrically-measured thin liquid film profiles, between the top of the bubble and the solid wall, was also in excellent agreement with the GNS profiles for the case of mobile bubble bouncing from a no-slip solid wall.

Here, we extend the above discussed bubbles bouncing from the flat glass interface investigation by measuring the free-rising bubble bouncing from mica, HOPG, and PTFE interfaces. In this way, we can compare the bouncing strength in water from two hydrophilic smooth interfaces, mica, and glass, with bouncing from two hydrophobic smooth interfaces, HOPG and PTFE. A stronger bounce of the bubbles from the hydrophobic surface compared to the hydrophilic surfaces could indicate an effective water slip on the hydrophobic surfaces, as the Pawliszak et al. study has claimed [27].

Video 2 compares the bouncing of identical size $D = 1.10$ mm bubbles from the hydrophilic glass surface and the strongly hydrophobic PTFE surface. In the same video, the bouncing is contrasted with the bouncing results using the GNS, for both the no-slip and free-slip wall cases. Video 3 shows another example comparing the bouncing of $D = 1.30$ mm bubbles from the hydrophilic mica surface with the hydrophobic HOPG surface and GNS for no-slip and full-slip walls. Fig. 4a shows snapshots and Fig. 4b the bubble center-of-mass trajectories extracted from Video 2. Fig. 4c shows snapshots and Fig. 4d the bubble center-of-mass trajectories extracted from Video 3. As seen in both of these examples in Video 2, Video 3, and Fig. 4 the bubble bounce trajectories for the paired hydrophilic and hydrophobic surfaces are identical and in excellent agreement with GNS for the bouncing from a no-slip wall. At the same time, the GNS for the bounce trajectory from a free-slip wall predicts a stronger bounce by a factor of $b_{im}/b_m \approx 1.5$ for the $D = 1.10$ mm bubble and $b_{im}/b_m \approx 1.3$, for the $D = 1.30$ mm bubble. The GNS of bounces from a no-slip wall correctly predicts the bubble trajectory and the complex way the bubble shape changes when the bubble bounces from the interface [Video 2, Video 3].

The only observed difference between bubbles bouncing from hydrophobic and hydrophilic surfaces seen in our experiments was that after the initial sequence of bounces, the bubble is faster to coalescence with the hydrophobic surface, as is seen in Video 2 for the case of bubble bouncing from the PTFE. The faster coalescence of the bubbles on the hydrophobic surface is expected and can be due to the hydrophobic forces or surface nano-bubbles presented at the hydrophobic interfaces [36].

The same results, as demonstrated in Videos 2 and 3, were repeated for the entire range of bubble sizes, using the four different substrates. Fig. 5 summarizes multiple experimental results for all of the substrates, now presented as dimensionless bouncing amplitudes of the first bounce

(a) Video 2.

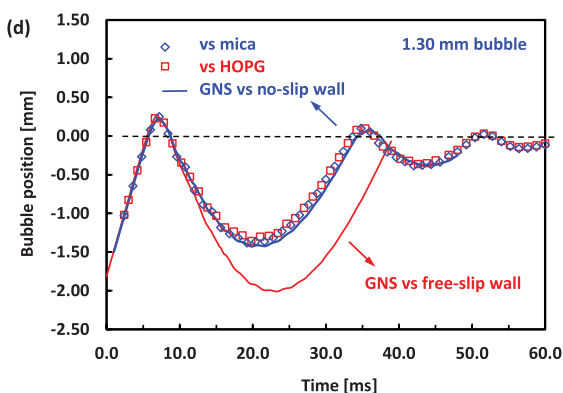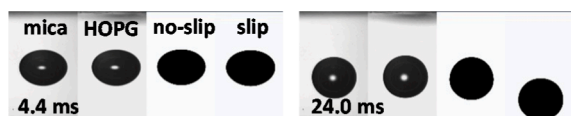**(b)**

(c) Video 3.

(d)
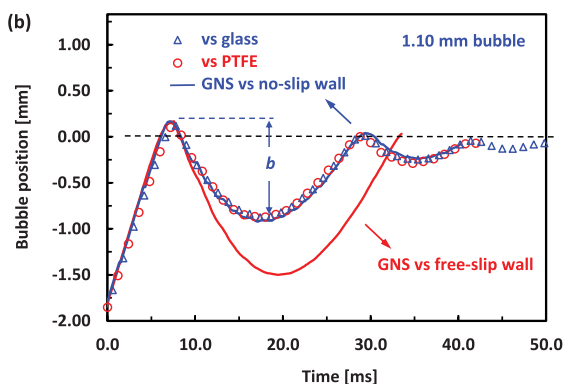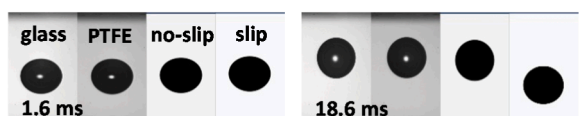
Fig. 4. (a) Snapshots from Video 2 illustrating the bounces of bubbles with a diameter of $D = 1.10$ mm, compared against GNS predictions. (b) Trajectory of the bubble center-of-mass extracted from Video 2, showing the bouncing from glass (blue triangles), PTFE (red circles), and GNS for no-slip wall (solid blue line) or free-slip wall (solid red line). (c) Snapshots from Video 3 paralleling the bounce of $D = 1.30$ mm bubbles with GNS predictions. (d) Trajectory of the bubble center-of-mass extracted from Video 3 for the case of bubble bouncing from mica (blue diamonds), HOPG (red squares), and GNS for no-slip wall (solid blue line) or free-slip wall (solid red line). (For interpretation of the references to color in this figure legend, the reader is referred to the web version of this article.)

b/D [Fig. 4b]. This is compared with the GNS predictions for bouncing from no-slip and free-slip interfaces. For the entire range of bubble sizes studied, from $D \approx 0.80$ to 1.40 mm, the first bounce amplitudes for all four substrates agree with each other and with the GNS results for the no-slip wall. In contrast, the GNS results for a free-slip wall predict significantly larger first bounce amplitudes. We note that the difference in bouncing amplitudes for free-slip compared to no-slip walls in the GNS simulations have a similar magnitude as the experimental results for bubbles bouncing from mobile and immobile water–air interfaces.
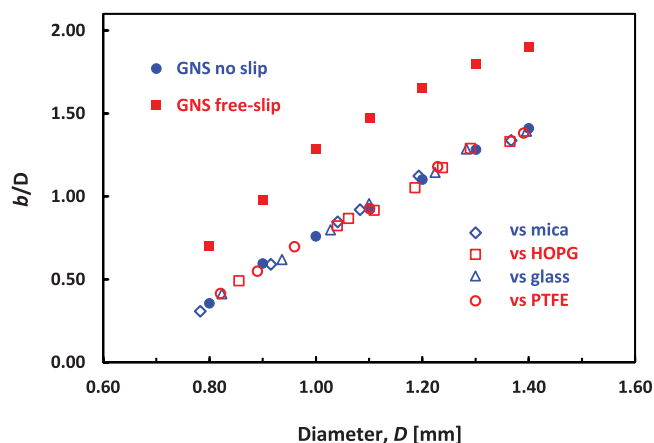

Fig. 5. Dimensionless first bounce distances, b/D, as measured in experiments with free-rising bubbles in pure water, bouncing from mica (empty blue diamonds), HOPG (empty red squares), glass (empty blue triangles), and PTFE (empty red circles) compared with GNS b/D values for bubbles bouncing from a no-slip wall (solid blue circles) or free-slip wall (solid red squares). (For interpretation of the references to color in this figure legend, the reader is referred to the web version of this article.)

In summary, our bubble-bounce experiments showed no evidence of water slip on the smooth hydrophobic surfaces investigated, HOPG and PTFE. The experiments for the bubbles bouncing from both hydrophobic and hydrophilic surfaces are in excellent agreement with each other and with the numerical simulations for bubbles bouncing from a no-slip flat wall. The agreement of bubble-bounce kinematics with the no-slip boundary condition on the wall is not surprising. In fact, all prior work we know of include numerical simulations by other groups [37] and analytical modeling, as for example the force-balance model developed by Manica et al. [38,39], show excellent agreement with the experimental data applying the no-slip boundary condition on the solid wall. Notably the Manica el al. [38] modeling demonstrates excellent no-slip wall agreement for bubbles bouncing from both Teflon and glass interfaces, using data from Kosior et al. [35].

Based on our experiments, numerical simulations, and prior analytical models, one can conclude that the recently observed decrease in the bubble bounce distance from hydrophilic surfaces in the work of Pawliszak et al. [27], is most probably due to contamination of the bubble from the biopolymers used to increase the substrate hydrophilicity. A direct comparison of our data with the data of Pawliszak et al. for the bubbles bouncing from a Teflon interface shows almost identical first bounce distance (for $D = 0.8$ mm; $d/D \approx 0.33$ in [27] and $d/D \approx 0.35$ in this work). This means that instead of an increase in the bubble bouncing distance due to slip on hydrophobic surfaces, this study measures a more than two-fold decrease in the bubble bounce distance when the surface is modified with the biopolymer. The only reasonable explanation for such a dramatic decrease in the bounce amplitude is contaminations by the biopolymer and related immobilization of the bubble interface by Marangoni stress effects [5,6]. A similar reduction in the bubble bounce amplitude, due to different levels of bubble contamination, has been demonstrated in the works of Manica et al., modeling experimental data for bubbles bouncing from glass surfaces [39,40].

The same approach used here to compare the water bubble bouncing from smooth solid hydrophilic and hydrophobic interfaces could also be applied for superhydrophobic surfaces, e.g. microstructure hydrophobic surfaces of water contact angle of more than 160°. When dipped in water the superhydrophobic surfaces sustain a thin air layer, referred to as a plastron. However, conducting reproducible bubble bounce experiments on microtextured surfaces is significantly more challenging than on flat solid surfaces due to several factors. First, the properties of the plastron depend on variables such as the type of the textured surface and the duration of its immersion in water. Second, an additional complication

is that bubbles tend to coalesce upon their first collision with the plastron, often without bouncing back. This phenomenon has been exploited in studies aiming to enhance rapid bubble coalescence and collection [41–44]. In a related study, Rapoport et al. [44], provides limited data suggesting that, while bubbles coalesce much faster on textured surfaces, in cases where a bubble does bounce back without coalescing, the bounce kinetics are not significantly different between flat and air-retaining microtextured surfaces. The identical bounce is not that surprising considering that the plastron layer is typically thin (microns or less) and remains pinned to the substrate. Using a similar super-hydrophobic coating as in the work of Rapoport et al. (Glaco by Soft 99 [45]) experiments with free-falling superhydrophobic spheres showed that the plastron-related partial-slip effects on the drag on a sphere became noticeable only at Reynolds numbers exceeding 10^5 [46]. In contrast, free-rising bubbles in pure water exhibit fully mobile behavior at Reynolds numbers above 100. Nevertheless, further detailed investigation into bubble bouncing on superhydrophobic surfaces is necessary to comprehensively evaluate the sensitivity of this approach in detecting slip effects on such surfaces.

3.4. GNS estimation of the shear rates

The magnitude of the shear rate and the related shear stress at the solid interfaces are a major factor that could determine the initiation of the liquid slip on a solid surface [8,9,15]. Here, we use the GNS results to estimate the shear rates on the flat interfaces during the bubble bounce. The shear rate γ, and shear stress, τ on the surface during the bubble bounces from the interface can be estimated as:

$$\gamma = u_{\mathrm{x}}^{\mathrm{b}}/h \tag{1}$$

$$\tau = \mu u_{\mathrm{x}}^{\mathrm{b}}/h \tag{2}$$

where μ is the dynamic viscosity of the liquid, $u_{\mathrm{x}}^{\mathrm{b}} = u_{\mathrm{x}}(y = h)$ is the fluid tangential velocity (parallel to the flat wall) at the bubble interface and h the thin liquid film thickness (Fig. 6a).

Video 4 is a GNS generated video that visualizes the tangential velocity field during the bouncing of a 1.30 mm bubble from the no-slip wall. Fig. 6 illustrates several snapshots from this video, zooming in on the thin liquid film formed during the bubble's first approach to the interface. Using the simulation data, we estimate that the maximum shear rate during this first bounce is about 30,000 s^{-1} and the shear stress is about 30 Pa (Fig. 6).

In AFM experiments, the approach velocity of the probe to the interfaces is typically lower than the bubble approach velocities in our experiments ($u_{\mathrm{x}} \sim$ μm/s (AFM) *vs.* cm/s (bubble)). However, because in AFM experiments the probe can be driven down to contact with the substrate ($h \sim$ nm (AFM) *vs.* μm (bubble)), shear rates can vary from about 10^1 to 10^5 s^{-1} [15]. In molecular dynamics simulations, a much higher shear rate is typically used $\gamma \sim 10^{11}$ s^{-1} [47]. Despite the comparable shear rates in AFM experiments and orders of magnitude higher shear rates used in simulations, the slip length is typically only a few to tens of nanometers. The low shear rates and expected slip-length magnitudes in the bubble bounce experiments further suggest that it is unlikely that any water slip effects could be detected in experiments on the bubble bouncing from solid surfaces.

4. Conclusions

The existence and the magnitude of the hydrodynamic slip of water on smooth hydrophobic surfaces has been long debated [7–17]. In most of these previous studies, such phenomena were expected in confined flow configurations, and the slip length could vary from several to tens of nanometers. In a recent study, the observed difference between bubbles bouncing from smooth hydrophobic surfaces (Teflon or graphite) and hydrophilic polymer-modified graphite was interpreted as
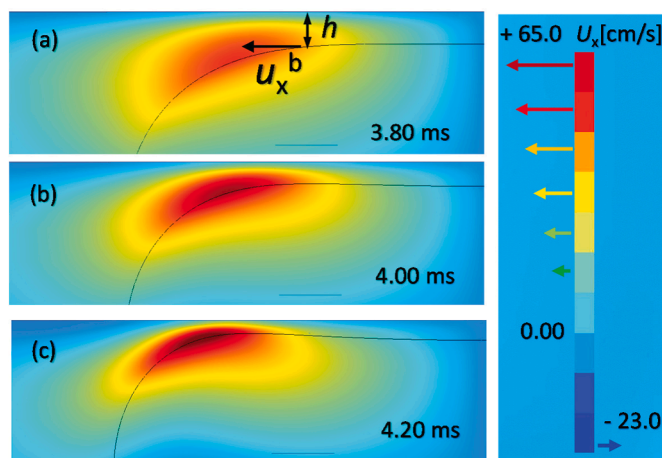

Fig. 6. Snapshots from Video 4 visualizing the tangential velocity field (parallel to the wall) for a 1.30 mm bubble bouncing from a no-slip wall. The snapshots are zoomed in on the thin liquid film during the first approach of the bubble to the interface at times 3.80 ms (a), 4.00 ms (b) and 4.20 ms (c). In the last panel, at time 4.20 ms, $u_{\mathrm{x}}^{\mathrm{b}} \approx 65.0$ cm/s, $h \approx 22$ μm, and $\gamma \approx 30,000$ s^{-1}. The color scale on the right shows the magnitude of the tangential velocity used in the video.

evidence of a significant water slip on the smooth hydrophobic surfaces [27].

To examine the possible water slip reported in this prior investigation, we compare the bouncing of free-rising mobile-interface bubbles from the smooth hydrophobic surfaces of Teflon or graphite with the bouncing from a smooth hydrophilic surface of glass or mica. Our experiments demonstrate that the bubbles bounce identically from the hydrophilic and hydrophobic surfaces for the entire range of bubble sizes studied, i.e. $D = 0.80$ to 1.40 mm. The experimental bouncing dynamics of the bubbles agree perfectly with numerical simulations of bubbles bouncing from a smooth no-slip wall. In contrast, simulations of the bubble bounce from a free-slip wall predict a much stronger bounce. Our study thus confirms the no-slip boundary conditions during the interaction of millimeter-range bubbles on smooth solid hydrophilic or hydrophobic surfaces. Future investigations can be directed to more complex hydrophobic surfaces such as hydrophobic polymer modified surfaces and plastron sustaining superhydrophobic surfaces.

Although the present study uses free-rising bubbles, we expect the no-slip boundary condition at the solid-water interface to hold for interaction in various practically important colloidal systems involving similar size range deformable bubbles, droplets, and solid colloidal particles [23,48].

CRediT authorship contribution statement

Ivan U. Vakarelski: Writing – original draft, Methodology, Investigation, Formal analysis, Data curation, Conceptualization. **Farrukh Kamoliddinov:** Software, Investigation, Data curation. **Sigurdur T. Thoroddsen:** Writing – review & editing, Supervision.

Declaration of competing interest

The authors declare that they have no known competing financial interests or personal relationships that could have appeared to influence the work reported in this paper.

Acknowledgments

Recovery and Resilience Plan of the Republic of Bulgaria, project SUMMIT BG-RRP-2.004-0008.

Appendix A. Supplementary data

Supplementary data (Supplementary Video 1–Video 4 and a file contiaing Supplementary Fig. S1–Fig. S3) to this article can be found online at https://doi.org/10.1016/j.jcis.2024.12.160.

Data availability

Data will be made available on request.

References

[1] B. Liu, R. Manica, Z. Xu, Q. Liu, The boundary condition at the air–liquid interface and its effect on film drainage between colliding bubbles, Curr. Opin. Colloid Interface Sci. 50 (2020) 101374.
[2] I.U. Vakarelski, F. Yang, S.T. Thoroddsen, Effects of interface mobility on the dynamics of colliding bubbles, Curr. Opin. Colloid Interface Sci. 57 (2022) 101540.
[3] H. Stone, A. Stroock, A. Ajdari, Engineering flows in small devices: Microfluidics toward a lab-on-a-chip, Annu. Rev. Fluid Mech. 36 (2004) 381–411.
[4] L. Bocquet, E. Charlaix, Nanofluidics, from bulk to interfaces, Chem. Soc. Rev. 39 (2010) 1073–1095.
[5] O. Manor, I.U. Vakarelski, X. Tang, S.J. O'Shea, G.W. Stevens, F. Grieser, R.R. Dagastine, D.Y.C. Chan, Hydrodynamic boundary conditions and dynamic forces between bubbles and surfaces, Phys. Rev. Lett. 101 (2008) 024501.
[6] B. Liu, R. Manica, Q. Liu, E. Klaseboer, Z. Xu, G. Xie, Coalescence of bubbles with mobile interfaces in water, Phys. Rev. Lett. 122 (2019) 194501.
[7] O.I. Vinogradova, Slippage of water over hydrophobic surfaces, Int. J. Miner. Process. 56 (1999) 31–60.
[8] V.S.J. Craig, C. Neto, D.R.M. Williams, Shear-dependent boundary slip in an aqueous Newtonian liquid, Phys. Rev. Lett. 87 (2001) 054504.
[9] C. Neto, D.R. Evans, E. Bonaccurso, H.-J. Butt, V.S.J. Craig, Boundary slip in Newtonian liquids: a review of experimental studies, Rep. Prog. Phys. 68 (2005) 2859–2897.
[10] D.M. Huang, C. Sendner, D. Horinek, R.R. Netz, L. Bocquet, Water slippage versus contact angle: a quasiuniversal relationship, Phys. Rev. Lett. 101 (2008) 226101.
[11] A. Maali, Y. Wang, B., Bhushan evidence of the no-slip boundary condition of water flow between hydrophilic surfaces using atomic force microscopy, Langmuir 25 (2009) 12002–12005.
[12] C.D.F. Honig, W.A. Ducker, Ducker no-slip hydrodynamic boundary condition for hydrophilic particles, Phys. Rev. Lett. 98 (2007) 028305.
[13] A.P. Bowles, C.D.F. Honig, W.A. Ducker, No-slip boundary condition for weak solid-liquid interactions, J. Phys. Chem. C 115 (2011) 8613–8621.
[14] L. Zhu, P. Attard, C. Neto, Reliable measurements of interfacial slip by colloid probe atomic force microscopy. II. Hydrodynamic force measurements, Langmuir 27 (2011) 6712–6719.
[15] L. Zhu, P. Attard, C. Neto, Reliable measurements of interfacial slip by colloid probe atomic force microscopy. III. Shear-rate-dependent slip, Langmuir 28 (2012) 3465–3473.
[16] A.P. Bowles, W.A. Ducker, Flow of water adjacent to smooth hydrophobic solids, J. Phys. Chem. C 117 (2013) 14007–14013.
[17] K. Ahmad, X. Zhao, Y. Pan, W. Wang, Y. Huang, Atomic force microscopy measurement of slip on smooth hydrophobic surfaces and possible artifacts, J. Phys. Chem. C 119 (2015) 12531–12537.
[18] E. Bonaccurso, H.-J. Butt, V.S.J. Craig, Surface roughness and hydrodynamic boundary slip of a Newtonian fluid in a completely wetting system, Phys. Rev. Lett. 90 (2003) 144501.
[19] T. Lee, E. Charrault, C. Neto, Interfacial slip on rough, patterned and soft surfaces: A review of experiments and simulations, Adv. Colloid Interface Sci. 210 (2014) 21–38.
[20] A. Busse, N.D. Sandham, G. McHale, M.I. Newton, Change in drag, apparent slip and optimum air layer thickness for laminar flow over an idealised superhydrophobic surface, J. Fluid Mech. 727 (2013) 488–508.
[21] T. Jung, H. Choi, J. Kim, Effects of the air layer of an idealized superhydrophobic surface on the slip length and skin-friction drag, J. Fluid Mech. 790 (2016) R1.
[22] J.D. Berry, I.U. Vakarelski, D.Y.C. Chan, S.T. Thoroddsen, Navier slip model of drag reduction by Leidenfrost vapor layers, Phys. Fluids 29 (2017) 107104.
[23] I.U. Vakarelski, F. Yang, Y.S. Tian, E.Q. Li, D.Y.C. Chan, S.T. Thoroddsen, Mobile-surface bubbles and droplets coalesce faster but bounce stronger, Sci. Adv. 5 (2019) eaaw4292.
[24] I.U. Vakarelski, F. Yang, S.T. Thoroddsen, Free-rising bubbles bounce more strongly from mobile than from immobile water-air interfaces, Langmuir 36 (2020) 5908–5918.
[25] I.U. Vakarelski, F. Kamoliddinov, S.T. Thoroddsen, Bubble mobility in seawater during free-rise, bouncing, and coalescences with the seawater-air interface, Colloids Surf. A 651 (2022) 129775.
[26] I.U. Vakarelski, K.R. Langley, F. Yang, S.T. Thoroddsen, Interferometry and simulation of the thin liquid film between a free-rising bubble and a glass substrate, Langmuir 38 (2022) 2363–2371.
[27] P. Pawliszak, A. Beheshti, A. Møller, A. Blencowe, D.A. Beattie, M. Krasowska, Increasing surface hydrophilicity with biopolymers: a combined single bubble collision, QCM-D and AFM study, J. Colloid Interface Sci. 667 (2024) 393–402.
[28] A. Milling, P. Mulvaney, I. Larson, Direct measurement of repulsive van der Waals interactions using an atomic force, Microscope 180 (1996) 460–465.
[29] S. Popinet, GERRIS FLOW SOLVER, http://gfs.sf.net.
[30] S. Popinet, An accurate adaptive solver for surface-tension-driven interfacial flows, J. Comput. Phys. 228 (2009) 5838–5866.
[31] D. Fuster, G. Agbaglah, C. Josserand, S. Popinet, S. Zaleski, Numerical simulation of droplets, bubbles and waves: state of the art, Fluid Dyn. Res. 41 (2009) 065001.
[32] X. Chen, Y. Sun, C. Xue, Y. Yu, G. Hu, Tunable structures of compound droplets formed by collision of immiscible microdroplets, Microfluid. Nanofluid 21 (2017) 109.
[33] D.W. Moore, The velocity of rise of distorted gas bubbles in a liquid of small viscosity, J. Fluid Mech. 23 (1965) 749–766.
[34] R. Manica, E. Klaseboer, D.Y.C. Chan, The impact and bounce of air bubbles at a flat fluid interface, Soft Matter 12 (2016) 3271–3282.
[35] D. Kosior, J. Zawala, M. Krasowska, K. Malysa, Influence of n-octanol on the bubble impact velocity, bouncing and the three phase contact formation at hydrophobic solid surfaces, Colloids Surf A 441 (2014) 788–795.
[36] R.F. Tabor, F. Grieser, R.R. Dagastine, D.Y.C. Chan, The hydrophobic force: measurements and methods, Phys. Chem. Chem. Phys. 16 (2014) 18065–18075.
[37] A. Albadawi, D.B. Donoghue, A.J. Robinson, D.B. Murray, Y.M.C. Delauré, On the assessment of a VOF based compressive interface capturing scheme for the analysis of bubble impact on and bounce from a flat horizontal surface, Int. J. Multiphase Flow 65 (2014) 82–97.
[38] R. Manica, E. Klaseboer, D.Y.C. Chan, Force balance model for bubble rise, impact, and bounce from solid surfaces, Langmuir 31 (2015) 6763–6772.
[39] R. Manica, E. Klaseboer, D.Y.C. Chan, The hydrodynamics of bubble rise and impact with solid surfaces, Adv. Colloid Interface Sci. 235 (2016) 214–232.
[40] R. Manica, M.H.W. Hendrix, R. Gupta, E. Klaseboer, C.-D. Ohl, D.Y.C. Chan, Effects of hydrodynamic film boundary conditions on bubble–wall impact, Soft Matter 9 (2013) 9755–9758.
[41] J. Wang, Y. Zheng, F.-Q. Nie, J. Zhai, L. Jiang, Air bubble bursting effect of lotus leaf, Langmuir 25 (2009) 14129–14134.
[42] H. Maleprade, C. Clanet, D. Quéré, Spreading of bubbles after contacting the lower side of an aerophilic slide immersed in water, Phys. Rev. Lett. 117 (2016) 094501.
[43] K.I. Hegner, W.S.Y. Wong, D. Vollmer, Ultrafast bubble bursting by superamphiphobic coatings, Adv. Mater. 33 (2021) 2101855.
[44] L. Rapoport, T. Emmerich, K.K. Varanasi, Capturing bubbles and preventing foam using aerophilic surfaces, Adv. Mater. Interfaces 7 (2020) 1901599.
[45] I.U. Vakarelski, N.A. Patankar, J.O. Marston, D.Y.C. Chan, S.T. Thoroddsen, Stabilization of Leidenfrost vapour layer by textured superhydrophobic surfaces, Nature 489 (2012) 274–277.
[46] A. Jetly, I.U. Vakarelski, S.T. Thoroddsen, Drag crisis moderation by thin air layers sustained on superhydrophobic spheres falling in water, Soft Matter 14 (2018) 1608–1613.
[47] M. Sega, M. Sbragaglia, L. Biferale, S. Succi, The importance of chemical potential in the determination of water slip in nanochannels, Eur. Phys. J. E 38 (2015) 127.
[48] I.U. Vakarelski, F. Kamoliddinov, S.T. Thoroddsen, Why bubbles coalesce faster than droplets: The effects of interface mobility and surface charge, Langmuir 40 (2024) 11340–11351.